J Electr Eng Technol Vol. 8, No. 2: 262-270, 2013
http://dx.doi.org/10.5370/JEET.2013.8.2.262

ISSN(Print) 1975-0102
ISSN(Online) 2093-7423

A Boundary Protection for Power Distribution Line Based on Equivalent Boundary Effect

Zhang Xin† and Mu Long-hua*

Abstract – A boundary protection method for power distribution line based on equivalent boundary effect is presented in this paper. In the proposed scheme, the equivalent resonance component with a certain central frequency is sleeve-mounted at the beginning of protected zone. The 'Line Boundary' is built by using boundary effect, which is created by introducing impedance in the primary-side of line. The 'Line Boundary' is significantly different from line wave impedance. Therefore, the boundary protection principle can be applied to power distribution line without line traps. To analyze the frequency characteristic corresponding to traveling-waves of introducing impedance in the primary-side of line, distributed parameters model of equivalent resonance component is established. The results of PSCAD/EMTDC simulation prove the obvious difference of voltage high frequency component between internal faults and external faults due to equivalent resonance component, and validate the scheme.

Keywords: Equivalent boundary effect, Equivalent resonance component, Power distribution line, Boundary protection

1. Introduction

Now protection principles based on power frequency information have been widely applied to distribution lines. For determining fault zone, many methods have been developed, including stage current protection and fiber differential protection. Such methods have many dis-advantages, such as long time consumption for handling faults and higher quality requirement for communication. Therefore, they could not ensure qualified reliability of supply.

Since 1990s, single-ended transient protection scheme has been used in high voltage and EHV transmission lines [1-9]. References [1-3] proposed a new single-ended transient protection scheme based on high frequency signals, which generated on a transmission line under fault conditions. The method hinged on utilizing power line carrier traps which are often used as part of line communication systems for transmitting high frequency signals from one end of the transmission line to the other. The line traps, which are almost transparent at power frequency, act as attenuators over a small band of high frequency. Thus, the traps confine the fault-generated high frequency signals to the protected zone. The concept of "Boundary Protection" is proposed [4]; the influence caused by various types of boundary resistance to transient signals is analyzed [5-6], which proves the existence of boundary effect on both sides.

† Corresponding Author: Dept. of Electrical Engineering, Tongji University, China.(zhangxin19791123@hotmail.com)
* Dept. of Electrical Engineering, Tongji University, China. (lhmu@ tongji.edu.cn)
Received: June 6, 2012; Accepted: October 9, 2012

Boundary protection of transmission line provides a new solution for protection of distribution line. In this solution, line traps are needed to strengthen the influence on high frequency component of fault signals. However, line traps are not frequently equipped in distribution lines. The absence of the line traps limits the application of boundary protection in distribution line.

A boundary protection scheme based on equivalent boundary effect and the wavelet energy spectrum is proposed in this paper. In this scheme, equivalent resonance component (ERC) with a certain central frequency is sleeve-mounted at the beginning of protected zone, which can change the transmission feature of transient signal in line boundary. With this idea, the internal and external faults could be distinguished, and then fast protection of distribution line is expected to be implemented.

2. Line Boundary Analysis Based on Equivalent Boundary Effect

2.1 Principle of equivalent boundary effect

Resonant circuit has significant attenuation on transient signal near to the center frequency, but no essential effect on signals of other bands away from center frequency. Based on this, an effective boundary effect could be created. The method is to sleeve-mount the equivalent resonance components with the same center frequency at the beginning of protected zones.

In the existed distribution network, the equivalent resonance component consists of Rogowski coil and relevant

load circuits. To analyze the response of introducing impedance to high frequency transient signal, the distributed parameter model of the equivalent resonant component is introduced in Fig.1 [10-11].
where

$R_0^{'}$ distributed windings' wire internal resistance;

$L_0^{'}$ distributed windings' self-inductance;

$C_0^{'}$ distributed windings' stray capacitance to shield;

Z_m impedance of the coil load;

$M^{'}$ distributed mutual inductance between windings of the coil and the cable's conductor.

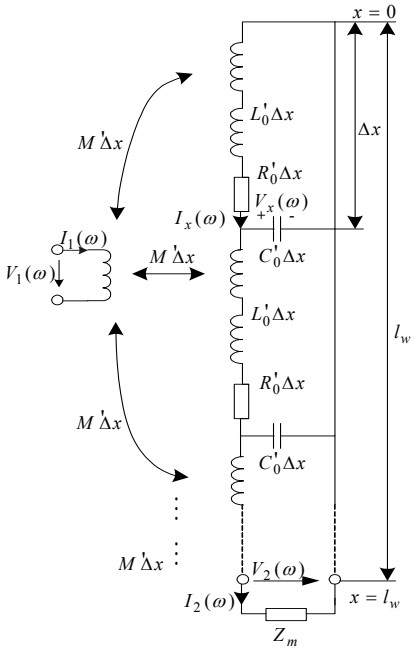

Fig. 1 Distributed parameters model of equivalent resonance component

Distributed stray capacitance among the turns is neglected.

At any point in the windings, the following established equations always work.

$$\frac{dV_x(\omega)}{dx} = -Z_S I_x(\omega) + j\omega M^{'} I_1(\omega) \tag{1}$$

$$\frac{dI_x(\omega)}{dx} = -j\omega C_0^{'} V_x(\omega) \tag{2}$$

where

$$Z_S = R_0^{'} + j\omega L_0^{'} \tag{3}$$

The general solution of the simultaneous differential equations formed by (1) and (2) are

$$V_x(\omega) = V_0^{+}(\omega)e^{-\gamma x} + V_0^{-}(\omega)e^{+\gamma x} \tag{4}$$

$$I_x(\omega) = \frac{V_0^{+}(\omega)e^{-\gamma x}}{Z_0} - \frac{V_0^{-}(\omega)e^{+\gamma x}}{Z_0} + \frac{j\omega M^{'} I_1(\omega)}{Z_S} \tag{5}$$

Where
propagation constant:

$$\gamma = \sqrt{(R_0^{'} + j\omega L_0^{'}) j\omega C_0^{'}} \tag{6}$$

wave impedance:

$$Z_0 = \sqrt{(R_0^{'} + j\omega L_0^{'}) / j\omega C_0^{'}} \ . \tag{7}$$

Applying boundary conditions

$$\begin{aligned} V_{x=0}(\omega) &= 0 \\ V_{x=l_w}(\omega) &= Z_m I_{x=l_w}(\omega) \end{aligned} \tag{8}$$

Yields

$$\begin{aligned} V_0^{+}(\omega) &= -V_0^{-}(\omega) \\ V_0^{+}(\omega) &= -\frac{j\omega M^{'} I_1(\omega) Z_m Z_0}{2Z_S(Z_0 \sinh(\gamma l_w) + Z_m \cosh(\gamma l_w))} \end{aligned} \tag{9}$$

The output current of the Rogowski coil $I_2(\omega)$, i.e.

$$I_2(\omega) = I_{x=l_w}(\omega) = \frac{j\omega M^{'} I_1(\omega) Z_0 \sinh(\gamma l_w)}{Z_S(Z_0 \sinh(\gamma l_w) + Z_m \cosh(\gamma l_w))} \tag{10}$$

Introducing impedance of the primary-side $Z_T^{'}$ is obtained by substituting (10) into $V_1(\omega) = j\omega M^{'} I_2(\omega)$, $V_1(\omega)$ is primary-side voltage of Rogowski coil, i.e.

$$Z_T^{'} = \frac{V_1(\omega)}{I_1(\omega)} = \frac{(j\omega M^{'})^2 Z_0 \sinh(\gamma l_w)}{Z_S(Z_0 \sinh(\gamma l_w) + Z_m \cosh(\gamma l_w))} \tag{11}$$

From (11), by choosing a proper Z_m, it is possible to make $Z_0 \sinh(\gamma l_w) = -Z_m \cosh(\gamma l_w)$. In this case, if there is equivalent parallel resonance near to a frequency, $Z_T^{'}$ can be substantial to constitute the boundary of line.

The equivalent resonance component adopts Rogowski coil with circular cross-section frame. The distance from center of frame cross-section to the center of the skeleton A = 50 mm, frame cross-section radius B =10 mm, number of turns N = 2500, the winding wire diameter Φ = 0.3 mm. According to $L = \mu_0 N^2 (A - \sqrt{A^2 - B^2})$, $M = \mu_0 N (A - \sqrt{A^2 - B^2})$ and the bridge measurement, the self-inductance of coil L_0 = 9.646mH, mutual inductance M =

3.8584μH, resistance R_0 =62.13Ω, stray capacitance C_0 = 0.12 nF. Meanwhile, the parameters of winding per unit length can be obtained: $L_0^{'}$ = 0.1237 mH/m, $M^{'}$ = 0.0495 μH/m, $R_0^{'}$ =0.7965 Ω/m, $C_0^{'}$ =1.5384 pF/m.

When $Z_m = R + j\omega C$, where R = 8965.8 Ω, C = 35.863 nF. At frequency $f \approx 80$ kHz, it is easy to get $Z_0 \sinh(\gamma l_w) \approx -Z_m \cosh(\gamma l_w)$, and the frequency characteristic of introducing impedance $Z_T^{'}$ is shown in Fig.2.

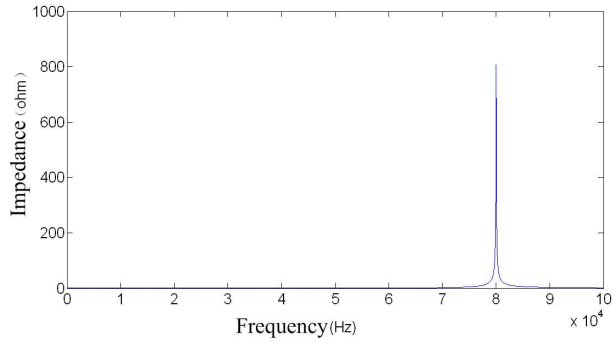

Fig. 2. Frequency characteristic of introducing impedance

From Fig. 2, near to the resonance center frequency f_0=80 kHz, the introducing impedance $Z_T^{'}$ appears high impedance. Based on this, this frequency band can be used as feature frequency band. also it has no influence on other frequency bands (especially power frequency), so the equivalent resonance component has no effect on the normal operation of distribution network.

2.2 Spectrum of refractive coefficient in the equivalent line boundary

For an external fault occurs in the forward direction or in the reverse direction, since equivalent resonance components are sleeve-mounted at the beginning of each protected zone, fault voltage traveling-waves are just different direction, but the attenuations of amplitudes in certain frequency band are similar through the equivalent resonance components. So an external fault occurs in the forward direction or in the reverse direction can be analyzed in the same way. The spectrum difference between the internal and external faults is mainly in the initial traveling-wave. The specific difference depends on the refractive coefficient of the line boundary. Many factors could affect the refractive coefficient, including line impedance, bus-to-bar capacitance, transient resistance and line traps, and so on.

Assuming that there are N outlets, besides the studied line, and all of their wave impedances are Z_c . With this assumption, the reflection model of distribution line boundary based on equivalent resonance component is presented in Fig.3, where C_s is bus-to-bar capacitance, $Z_T^{'}$ is the equivalent impedance of resonance component. Incident wave W_r spreads from line 1 to the bus M, and at the same time, producing reflected wave W_f , part of the incident wave spreads to the studied line through bus and produces refracted wave W_z , part of the incident wave spreads to other lines and produces refracted wave W_{z2} , …, W_{zn} ,. The reference directions of each traveling-wave, voltage and current are shown in Fig. 3.

According to traveling-wave theory and KVL, KCL theorem, the refractive coefficient of line boundary (K_z)[12] can be obtained by

$$K_z = \frac{W_z}{W_r} = \frac{2Z_c}{Z_c + (n + j\omega C_S Z_c)(Z_c + Z_T^{'})} \tag{12}$$

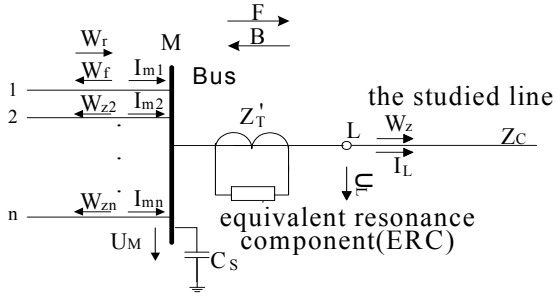

Fig. 3. Refractive model of line boundary based on equivalent resonance component

Substituting (11) into (12), the expression of K_z combined with equivalent resonance components is obtained. According to Section 2.1, parameters of resonance component are chosen. Other parameters are decided as Z_c =300Ω, C_s =0.002uF, n=2. The spectrum of refractive coefficient of line boundary is presented in Fig. 4.

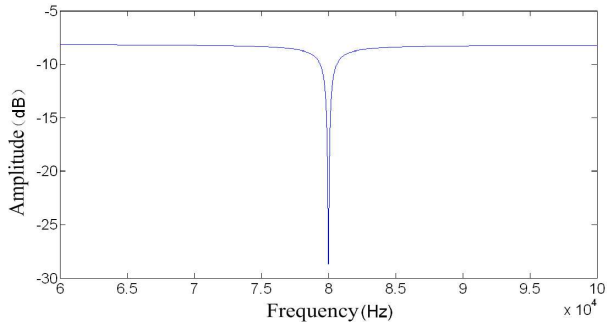

Fig. 4. Spectrum of refractive coefficient of line boundary based on equivalent resonance component

As shown in Fig. 4, the equivalent resonance component has significant effect on refractive coefficient of the line boundary. The K_z has big attenuation inside the feature frequency band (the biggest attenuation is about 30dB), which results in obvious difference of spectrum between internal and external fault.

3. The Principle of Boundary Protection Based on Equivalent Boundary Effect

The basic principle of boundary protection is that when external fault occurs, the attenuation of high frequency band (especially in band of line trap) of transient components generated by fault through line boundary is obvious, but for an internal fault, no attenuation of high frequency component results from the line boundary, so the fast protection could be built.

The equivalent resonance component is sleeve-mounted at the beginning boundary of distribution line, which could construct the boundary protection principle based on equivalent boundary effect: when fault occurs, all protection devices extract voltage components in the feature frequency band and select a voltage component far away from the resonance center frequency as a reference. Because the high frequency component of an external fault has been attenuated obviously through equivalent resonance component, while the high frequency component of an internal fault has not been attenuated, the ratio of voltage spectrum energy between the feature band and the reference band can be used as the boundary protection criterion of the distribution line.

4. Calculation of fault spectrum energy of distribution line

4.1 The choice of wavelet

Transient traveling-wave protection demands the analysis of spectrum of transient fault component in a specific time within a specific frequency band, thus the wavelet must have the following characteristsics:

1) In order to detect fault possibly, the wavelet has good time-frequency positioning effect. In other words, the smaller time-frequency window area is required;
2) In order to locate fault time accurately, the wavelet has linear phase;
3) In order to decompose rapidly, the wavelet must be orthogonal wavelet [13-14];
4) In order to obtain efficiently and rapidly, the wavelet must be compactly supported wavelet, or has rapid attenuation ability;
5) In order to detect the voltage crossing-zero fault, the wavelet has high possibly vanishing moment, because that vanishing moment represents the smoothness of wavelet and reflects the ability which detects high order singular points [18].

Therefore, Meyer wavelet is chosen to analyze the fault transient signal and the extract spectrum. Meyer wavelet is orthogonal wavelet, and has good time-frequency positioning effect and linear phase. Although Meyer wavelet is not compactly supported wavelet, it has rather fast attenuation ability. Especially, Meyer wavelet has infinite high vanishing moment, so it can detect the voltage crossing-zero fault.

A very useful implementation of Meyer wavelet transform is demonstrated in Fig. 5. Transient signal x (n) is passed through a highpass filter $G(\omega)$ and a lowpass filter $H(\omega)$. Then the outputs from both filters are decimated by 2 to obtain the wavelet coefficients and the scale coefficients at scale j (d_j and a_j). The scale coefficients are then sent to the next stage to repeat the procedure. Finally, the signal is decomposed at the expected scale. In the case shown in Fig. 5, if the sampling frequency is F, the signal extracted by d1 is between F/4 and F/2 of the frequency band. d2 extracts the signal between F/8 and F/4, d3 extracts the signal between F/16 and F/8, and a3 retains the rest of the signal between 0 and F/16.

When the actual sampling frequency is 250 kHz, after scale j=3 decomposition of the transient signal, wavelet coefficients d_1, d_2, d_3 and the scale coefficient a_3 can be obtained, the corresponding frequency band is 62.5-125kHz, 31.25-62.5kHz, 15.625-31.25kHz, 0-15.625kHz respectively.

In order to test the Meyer wavelet ability which detects the voltage crossing-zero fault, the paper gives an example. In case of the voltage crossing-zero fault, there are weak transient procedures of voltage, and the fault voltage is from one steady state to another. Assuming that fault time is t_0 , the signals are used to simulated the voltage in case of the voltage crossing-zero fault

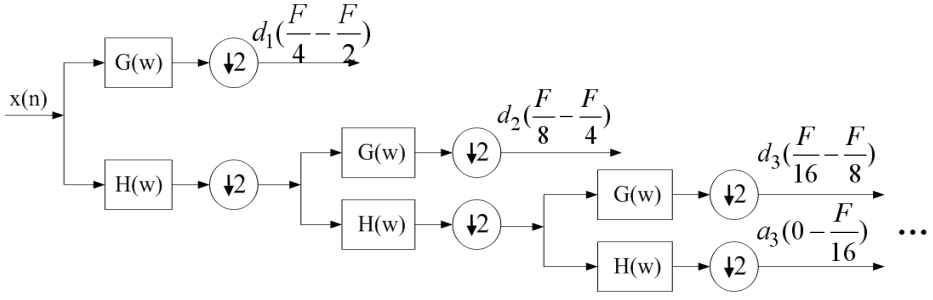

Fig. 5. Schematic diagram of binary wavelet transform signal decomposition

$$f(t)=\begin{cases} f_1(t)=A_1\cos(\mathbf{100}\pi t+\phi_1) & t\le t_0 \\ f_2(t)=A_2\cos(\mathbf{100}\pi t+\phi_2) & t>t_0 \end{cases} \tag{13}$$

When $t=t_0$, $f_1=f_2=0$, the waveforms of Meyer wavelet spectra are shown in Fig. 6.

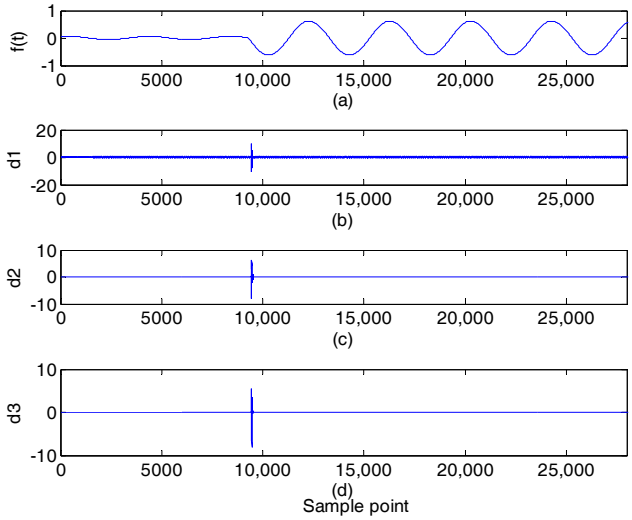

Fig. 6 Wavelet spectra of *f(t)* for Meyer wavelet transform. (a) *f(t)*. (b)d1.(c)d2. (d)d3.

As is shown in Fig.6, in case of the voltage crossing-zero fault, Meyer wavelet can detect the fault in scale 1 decomposition.

4.2. Phase-mode transformation

For distribution lines, due to the coupling between lines, traveling-waves in each phase transmission lines affect each other, and transient analysis is so complicated that each phase can't be analyzed directly. Therefore, using phase-mode transformation matrix, the three-phase coupled lines must be decoupled into three independent modulus networks, and then each network is analyzed separately. In this paper, Clark phase-mode transformation matrix is used as decoupling matrix and mode 1 voltage is used as input of boundary protection. Mode 1 voltage is shown as

$$\dot{U}_1=2\dot{U}_a-\dot{U}_b-\dot{U}_c \tag{14}$$

4.3. Calculation of the energy spectrum

According to Parseval Theorem, for the orthogonal wavelet, the energy of original signal is equivalent to the energy of expansion coefficient [16]. Corresponding to scale j, the high frequency energies of mode 1 signal are E_j, and low frequency energy mode 1 signal after the largest-scale decomposition is E_{S+1}. The energies corresponding to each scale are as follows

$$E_j=\sum_{k=1}^{N}|d_j(k)|^2\Delta T \tag{15}$$

$$E_{S+1}=\sum_{k=1}^{N}|a_S(k)|^2\Delta T \tag{16}$$

Normalizing (15) and (16)

$$E_j'=E_j\Big/\left(\sum_{j=1}^{S}E_j^2+E_{S+1}^2\right)^{0.5} \tag{17}$$

$$E_{S+1}'=E_{S+1}\Big/\left(\sum_{j=1}^{S}E_j^2+E_{S+1}^2\right)^{0.5} \tag{18}$$

Where

E_j the high frequency energies of mode 1 voltage , corresponding to scale j

E_{S+1} the low frequency energy mode 1 voltage after the largest-scale decomposition

N sampling points number

ΔT sampling time step

S the largest scale of wavelet decomposition

So as to narrate conveniently, if there is no special instruction, the upper sign of normalized transient energy are omitted.

4.4 Protection Criterion

According to boundary protection principle, the ratio of E_j to E_{S+1} of fault traveling-wave(λ) is considered as the protection criterion

$$\lambda=\frac{E_j}{E_{S+1}} \tag{19}$$

External faults are defined as reliability and no-action, the threshold is selected

$$\lambda_b=\max(\lambda_{ex}) \tag{20}$$

Where, λ_{ex} is the ratio of E_j to E_{S+1} when external fault occurs.

The center resonance frequency of the equivalent resonance component chosen in this paper is 80 kHz. Therefore, based on the frequency band information of wavelet transform, the ratio of E_1 to E_4 is used as the protection criterion. If $\lambda>\lambda_b$, it will be recognized as an internal fault.

5. PSCAD/EMTDC Simulation and Analysis

To verify the effectiveness of the proposed boundary

protection scheme based on the equivalent boundary effect, a local 35 kV distribution system is built with the software PSCAD/EMTDC. The ungrounded network shown in Fig. 7 is chosen for simulation. FD (Frequency Dependent) model is used in the distribution line; the line type is cable, and the distributed parameters of the line per unit length are: R0=0.178 Ω/km, L0=1.136 mH/km, C0=0.167 μF/km; the distances of MN, NP and NQ are all 10 km; the center resonance frequency of the equivalent resonance component is 80 kHz; the bus-to-bar capacitance is C_s; the sampling frequency of signal is 250 kHz, the sampling time is 2ms after faults occur, BU1-BU6 are protection devices of lines.

The simulation focuses on examining the protection performance of protection device(BU1) on the M side in Line MN, and MN is in its protection zone. The bus-to-bar capacitance after treatment varies from 2000 pF to 15000 pF [17]. In order to highlight the effect of the equivalent resonance component, C_s is assumed 2000pF in this simulation.

For example, the single phase to ground faults occur at the F1(internal point) and F3(external point). The fault signal is sampled 1 ms later than it happened. Each frequency band signal coefficient of Meyer wavelet extraction is shown in Fig. 8 and Fig. 9.

In Fig. 8 and Fig. 9, the corresponding frequency band of d1, d2, d3 and a3 is 62.5-125kHz, 31.25-62.5kHz, 15.625-31.25kHz, 0-15.625kHz. respectively. Comparing Fig. 8(d) with Fig. 9(d), there is obvious difference in amplitude of d1 coefficient, which frequency band is near to the equivalent resonance center frequency 80 kHz. It means that the wavelet coefficient in this band has been attenuated greatly through line boundary. Otherwise, amplitude of a3 coefficient in Fig. 8 (e) and Fig. 9 (e) have not changed much. From that, internal and external faults can be distinguished by the energy ratio λ.

Considering different fault conditions, simulation of sampling signal of BU, voltage traveling-wave boundary protection device, is carried out and the results are shown in Table 1~Table 3, in which F1~F6 represent different fault locations, CG, BCG, ABCG BC ABC represent C-phase-to-ground fault, double-phase-to-ground fault, three-phase-to-ground fault, double phase short circuit fault and three phase short circuit fault respectively.

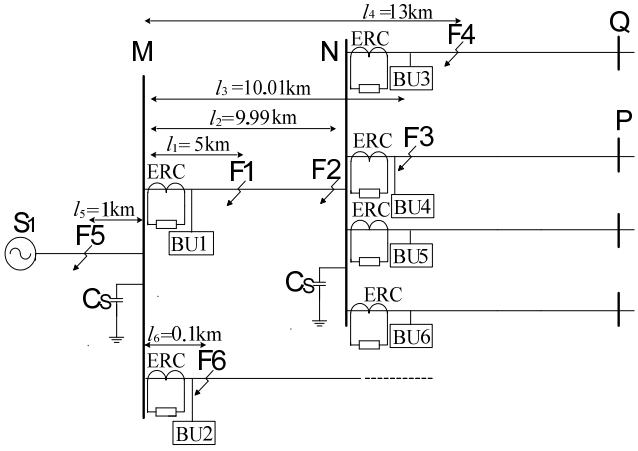

Fig. 7. Boundary protection simulation model based on Wavelet energy spectrum

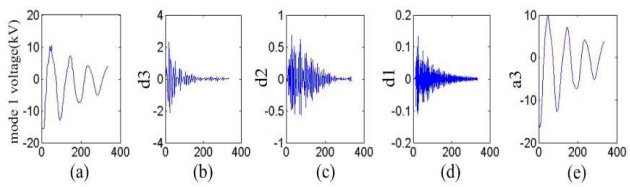

Fig. 8. CG external fault. (a) Model 1 voltage. (b) d3. (c) d2. (d) d1. (e) a3.

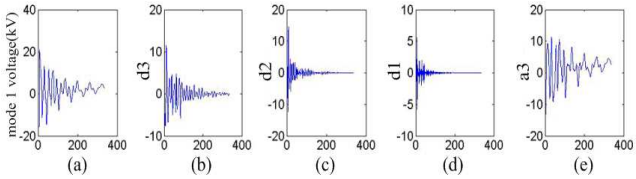

Fig. 9. CG internal fault. (a) Model 1 voltage. (b) d3. (c) d2. (d) d1. (e) a3

Table 1. Simulation results of energy ratio on bus M in case of internal faults

Rg=0Ω, Different fault angles			E_1	E_4	E_1/E_4
Internal Fault (F1 point)	0°	F1(CG)	0.0124	0.9802	0.0127
		F1(BCG)	0.0136	0.9793	0.0139
		F1(BC)	0.0119	0.9841	0.0121
		F1(ABCG)	0.0138	0.9775	0.0141
		F1(ABC)	0.0132	0.9795	0.0135
	45°	F1(CG)	0.0315	0.9663	0.0326
		F1(BCG)	0.0312	0.9664	0.0323
		F1(BC)	0.0317	0.9659	0.0328
		F1(ABCG)	0.0303	0.9674	0.0313
		F1(ABC)	0.0301	0.9675	0.0311
	90°	F1(CG)	0.0326	0.9602	0.0340
		F1(BCG)	0.0328	0.9601	0.0342
		F1(BC)	0.0331	0.9598	0.0345
		F1(ABCG)	0.0327	0.9601	0.0341
		F1(ABC)	0.0325	0.9602	0.0338
Internal Fault (F2 point)	0°	F2(CG)	0.0118	0.9820	0.0120
		F2(BCG)	0.0127	0.9804	0.0130
		F2(BC)	0.0102	0.9863	0.0103
		F2(ABCG)	0.0128	0.9804	0.0131
		F2(ABC)	0.0127	0.9804	0.0130
	45°	F2(CG)	0.0305	0.9671	0.0315
		F2(BCG)	0.0299	0.9679	0.0309
		F2(BC)	0.0295	0.9683	0.0305
		F2(ABCG)	0.0280	0.9702	0.0289
		F2(ABC)	0.0282	0.9703	0.0291
	90°	F2(CG)	0.0317	0.9659	0.0328
		F2(BCG)	0.0310	0.9667	0.0321
		F2(BC)	0.0306	0.9674	0.0316
		F2(ABCG)	0.0298	0.9679	0.0308
		F2(ABC)	0.0297	0.9680	0.0307

Table 4 shows λ, the energy ratio of the M side in case of CG at F1 point, when fault resistance changes, and fault initial angle is 45°. With increasing values of fault resistance, as is shown in Table 4, the energy ratio of the M side decreases, which is because the increase of fault resistance causes the decrease of fault initial voltage traveling-wave.

According to the simulation results of Table 1~ Table 4, in external faults, the maximum value of λ_{ex} occurs when double-phase-to-ground fault happens, and $\max\{\lambda_{ex}\} = \mathbf{5.62}e-\mathbf{5}$. According to (19), the threshold λ_b is $\mathbf{5.62}e-\mathbf{5}$.

When $\lambda = E_1 / E_4 > \lambda_b$, it is considered as internal faults.

It should be pointed that differences between voltage traveling-wave energy of internal faults and external faults depend on the refractive coefficient of line boundary. So the value of λ_b is related to line parameters and parameters of equivalent resonance components. If line parameters are changed, it could mean that wave impedances Z_C of the lines . We can tune the parameters of equivalent resonance components, including R and C, so impedance of the primary-side $Z_T^{'}$ is changed. According to (12), appropriate accommodation about $Z_T^{'}$ could create similar attenuation of refractive coefficient even when line parameters change.

Table 2. Simulation results of energy ratio on bus M in case of external faults in positive direction

Rg=0Ω, Different fault angles			E_1	E_4	E_1/E_4
External Fault in positive direction (F3 point)	0°	F3(CG)	8.65 e-6	1.0000	8.65 e-6
		F3(BCG)	1.37 e-5	1.0000	1.37 e-5
		F3(BC)	1.32 e-5	1.0000	1.32 e-5
		F3(ABCG)	1.27 e-5	1.0000	1.27 e-5
		F3(ABC)	1.35 e-5	1.0000	1.35 e-5
	45°	F3(CG)	2.77 e-5	1.0000	2.77 e-5
		F3(BCG)	5.56 e-5	1.0000	5.56 e-5
		F3(BC)	5.57 e-5	1.0000	5.57 e-5
		F3(ABCG)	3.02 e-5	1.0000	3.02 e-5
		F3(ABC)	3.06 e-5	1.0000	3.06 e-5
	90°	F3(CG)	3.03 e-5	1.0000	3.03 e-5
		F3(BCG)	5.62 e-5	1.0000	5.62 e-5
		F3(BC)	5.62 e-5	1.0000	5.62 e-5
		F3(ABCG)	3.21 e-5	1.0000	3.21 e-5
		F3(ABC)	3.28 e-5	1.0000	3.28 e-5
External Fault in positive direction (F4 point)	0°	F4(CG)	1.59 e-5	1.0000	1.59 e-5
		F4(BCG)	1.53 e-5	1.0000	1.53 e-5
		F4(BC)	1.06 e-5	1.0000	1.06 e-5
		F4(ABCG)	1.11 e-5	1.0000	1.11 e-5
		F4(ABC)	1.83 e-5	1.0000	1.83 e-5
	45°	F4(CG)	4.06 e-5	1.0000	4.06 e-5
		F4(BCG)	4.11 e-5	1.0000	4.11 e-5
		F4(BC)	4.03 e-5	1.0000	4.03 e-5
		F4(ABCG)	3.98e-5	1.0000	3.98e-5
		F4(ABC)	4.01 e-5	1.0000	4.01 e-5
	90°	F4(CG)	4.78 e-5	1.0000	4.78 e-5
		F4(BCG)	5.02 e-5	1.0000	5.02 e-5
		F4(BC)	4.98 e-5	1.0000	4.98 e-5
		F4(ABCG)	5.08e-5	1.0000	5.08e-5
		F4(ABC)	5.10 e-5	1.0000	5.10 e-5

In engineering applications, for different distribution lines, if line parameters are knowable, the value of protection threshold λ_b could be considered equal to or approximately equal to a fixed value by tuning the parameters of equivalent resonance components, which can ensure the versatility of the protection device.

Since the wavelet transform is very sensitive to the mutation of signal, fault initial angles will not affect the accuracy of protection criterion. Table 1~Table 3 show that the simulation results of λ, the energy ratio of the M side in different initial phase angles when faults occur. As is shown in Table 1~ Table 3, the initial phase angles have no influence on the determination of the fault location. Meanwhile, as is shown in Table 4, even fault resistance is very high (1 kΩ), λ is still bigger than the threshold.

Table 5 shows the results of BU1 at M point and BU4 at N point in case of BCG at F3 point, when fault resistance changes, and fault initial angle is 45°. As is shown in Table 5, both sides of bus can clearly distinguish internal faults and external faults.

Table 3. Simulation results of energy ratio on bus M in case of external faults in diverse direction

Rg=0Ω, Different fault angles			E_1	E_4	E_1/E_4
External Fault in diverse direction (F5 point)	0°	F5(CG)	1.21 e-5	1.0000	1.21 e-5
		F5(BCG)	1.02 e-5	1.0000	1.02 e-5
		F5(BC)	1.03 e-5	1.0000	1.03 e-5
		F5(ABCG)	9.96 e-6	1.0000	9.96 e-6
		F5(ABC)	1.02 e-5	1.0000	1.02 e-5
	45°	F5(CG)	3.96 e-5	1.0000	3.96 e-5
		F5(BCG)	3.25 e-5	1.0000	3.25 e-5
		F5(BC)	3.27 e-5	1.0000	3.27 e-5
		F5(ABCG)	3.16 e-5	1.0000	3.16 e-5
		F5(ABC)	3.18 e-5	1.0000	3.18 e-5
	90°	F5(CG)	4.03 e-5	1.0000	4.03 e-5
		F5(BCG)	3.97 e-5	1.0000	3.97 e-5
		F5(BC)	3.85 e-5	1.0000	3.85 e-5
		F5(ABCG)	3.92 e-5	1.0000	3.92 e-5
		F5(ABC)	3.95 e-5	1.0000	3.95 e-5
External Fault in diverse direction (F6 point)	0°	F6(CG)	6.85 e-6	1.0000	6.85 e-6
		F6(BCG)	6.23 e-6	1.0000	6.23 e-6
		F6(BC)	5.98 e-6	1.0000	5.98 e-6
		F6(ABCG)	5.96 e-6	1.0000	5.96 e-6
		F6(ABC)	5.94 e-6	1.0000	5.94 e-6
	45°	F6(CG)	2.13 e-5	1.0000	2.13 e-5
		F6(BCG)	2.25 e-5	1.0000	2.25 e-5
		F6(BC)	2.31 e-5	1.0000	2.31 e-5
		F6(ABCG)	2.30 e-5	1.0000	2.30 e-5
		F6(ABC)	2.31 e-5	1.0000	2.31 e-5
	90°	F6(CG)	2.54 e-5	1.0000	2.54 e-5
		F6(BCG)	2.63 e-5	1.0000	2.63 e-5
		F6(BC)	2.61 e-5	1.0000	2.61 e-5
		F6(ABCG)	2.59e-5	1.0000	2.59e-5
		F6(ABC)	2.58 e-5	1.0000	2.58 e-5

Table 4. Transient energy ratio of different fault resistance

Fault Resistance/Ω	E_1	E_4	E_1/E_4
0	0.0315	0.9663	0.0326
50	0.0157	0.9948	0.0149
1000	2.08e-4	1.0000	1.97 e-4

Table 5. Transient energy ratio of different BU

	Rg/Ω	E_1	E_4	E_1/E_4	Results
BU1	0	5.56 e-5	1.0000	5.56 e-5	External fault
	5	5.11 e-5	1.0000	5.11 e-5	External fault
	15	4.98 e-5	1.0000	4.98 e-5	External fault
	30	4.57 e-5	1.0000	4.57 e-5	External fault
BU4	0	0.0315	0.9663	0.0326	Internal fault
	5	0.0301	0.9675	0.0311	Internal fault
	15	0.0289	0.9707	0.0298	Internal fault
	30	0.0213	0.9765	0.0218	Internal fault

Table 6 shows the results of BU1、BU2、BU3 and BU4 in case of BCG at different fault locations, when fault resistance is 0Ω, and fault initial angle is 45°. As is shown in Table 6, each BU can clearly distinguish internal faults and external faults.

Table 6. Transient energy ratio of different BU with different fault locations

		E_1	E_4	E_1/E_4	Results
BU1	F1	0.0312	0.9664	0.0323	Internal fault
	F2	0.0299	0.9679	0.0309	Internal fault
	F3	5.56 e-5	1.0000	5.56 e-5	External fault
	F4	4.11 e-5	1.0000	4.11 e-5	External fault
	F5	3.25 e-5	1.0000	3.25 e-5	External fault
BU2	F1	2.13 e-5	1.0000	2.13 e-5	External fault
	F2	1.97 e-5	1.0000	1.97 e-5	External fault
	F3	1.22 e-5	1.0000	1.22 e-5	External fault
	F4	1.15 e-5	1.0000	1.15 e-5	External fault
	F5	5.12 e-5	1.0000	5.12 e-5	External fault
BU3	F1	4.36 e-5	1.0000	4.36 e-5	External fault
	F2	5.25 e-5	1.0000	5.25 e-5	External fault
	F3	2.06 e-5	1.0000	2.06 e-5	External fault
	F4	0.0313	0.9664	0.0324	Internal fault
	F5	2.98 e-5	1.0000	2.98 e-5	External fault
BU4	F1	4.39 e-5	1.0000	4.39 e-5	External fault
	F2	5.07 e-5	1.0000	5.07 e-5	External fault
	F3	0.0311	0.9667	0.0322	Internal fault
	F4	2.15 e-5	1.0000	2.15 e-5	External fault
	F5	2.11 e-5	1.0000	2.11 e-5	External fault

In China, the distribution systems with 3~60kV almost use non-effectively grounding mode, including ungrounded mode, arc-extinguishing-coil grounded mode and high resistance grounded mode. Table 7 shows the energy ratio of the M side in case of CG at F1 and F3 point, when neutral grounding changes, and fault initial angle is 45°. As is shown in Table 7, whatever neutral grounding, the difference of transient energy ratio between internal fault and external fault is obvious, and BU1 can distinguish internal fault or external fault.

Table 7. Transient energy ratio of different neutral grounding

Fault Location	neutral grounding	E_1	E_4	E_1/E_4
F1	ungrounded	0.0315	0.9663	0.0326
	arc-extinguishing-coil	0.0227	0.9724	0.0233
	high resistance	0.0312	0.9664	0.0323
F3	ungrounded	2.77 e-5	1.0000	2.77 e-5
	arc-extinguishing-coil	1.06 e-5	1.0000	1.06 e-5
	high resistance	2.65 e-5	1.0000	2.65 e-5

Table 1 to 7 and more simulation results show that:

1) For internal and external faults, high frequency energy characteristics of voltage traveling-wave are obviously different (especially near to the center frequency of the resonance component), and their energy characteristics of low frequency energy are little variation. According to the ratio of high frequency energy and low frequency transient energy $\lambda = E_1 / E_4$, internal and external faults can be discriminated correctly.
2) Types of faults, neutral grounding mode and the fault resistance will not affect the results of the distinguishing of internal and external faults.
3) Although there are weak transient signals when fault initial angle is 0°, Meyer wavelet can still detect high order singular points caused by faults. Fault initial angle will not affect the accuracy of the scheme.

6. Conclusions

Based on boundary protection principle, a boundary protection scheme for power distribution line based on equivalent boundary effect is presented in this paper. The features are as follows:

1) For solving the difficulty of applying the boundary protection principle to distribution lines without line traps, the equivalent resonance component with a certain central frequency is sleeve-mounted at the beginning of protected zone. Using introducing impedance in the primary side can create obvious boundary effect.
2) As for internal and external faults, their energies difference of voltage traveling-wave in the feature frequency band of the equivalent resonance component is the most obvious, so the energy ratio of the feature frequency band and the reference frequency band can be considered as the protection criteria.
3) Line parameters have great effect on the threshold λ_b, but when the system is determined, it is only needed to tune the parameters of the equivalent resonance components to get satisfying boundary effect, which can make the threshold λ_b similar to a fixed value to meet the requirement of versatility.
4) Fault conditions will not affect the results of the distinguishing of internal and external faults.

References

[1] A T Johns, RK Aggarwal, and Z Q Bo, "Non-unit protection technique for EHV transmission systems based on fault-generated noise, Part 1 - Signal measurement," *IEE Proc-Gener. Transm. Distrib*, Vol.

141, No. 2, pp. 133-140, 1994.

[2] A T Johns, RK Aggarwal, and Z Q Bo, "Non-unit protection technique for EHV transmission systems based on fault-generated noise, Part 2 - Signal processing," *IEE Proc-Gener. Transm. Distrib*, Vol. 141, No. 2, pp. 141-147, 1994.

[3] RK Aggarwal, A T Johns, and Z Q Bo, "Non-unit protection technique for EHV transmission systems based on fault-generated noise, Part 3 - engineering and HV laboratory testing," *IEE Proc-Gener. Transm. Distrib*, Vol. 143, No. 3, pp. 276-282, 1996.

[4] Chen Z, Bo Z Q, and Jiang F, *et al*, "A fault generated high frequency current transients based protection scheme for series compensated lines," *IEEE Power Engineering Society Winter Meeting*, Singapore: 2000.

[5] Zhang Baohui, Ha Hengxu, and Duan Jiandong, *et al*, "IEEE/PES Boundary Protection, A New Concept for Extra High Voltage Transmission Lines --- Part I: Spectrum Analysis of Fault Induced Transients," *Transmission and Distribution Conference and Exhibition: Asia and Pacific*, Dalian, China, 2005, pp. 1-5.

[6] Zhang Baohui, Ha Hengxu, and Duan Jiandong, *et al*, "IEEE/PES Boundary Protection, A New Concept for Extra High Voltage Transmission Lines --- Part II: Discriminative Criterions and Simulations," *Transmission and Distribution Conference and Exhibition: Asia and Pacific*, Dalian, China, 2005, pp. 1-6.

[7] Duan Jiandong, Jun Kuang, and Wu Shanshan, "Boundary Protection Algorithm Based on Phase Information of Improved Recursive Wavelet Transform for EHV Transmission Lines," *Power and Energy Engineering Conference, Asia-Pacific,* Wuhan, China, 2009, pp. 1-4.

[8] Li, M.X, Bo, Z.Q, and He, J.H, *et al*, "Simulation evaluation of an integrated boundary protection scheme," *IEEE Bucharest Power Tech Conference*, Bucharest, Romania, 2009, pp. 1-6.

[9] Xia Mingchao, Huang Yizhuang, and Zhao Woquan, "A novel protection algorithm for high voltage transmission line using multi-end transient current," *Proceedings of the CSEE*, Vol. 24, No. 2, pp. 39-42, 2004.

[10] Yi Liu, Fuchang Lin, and Qin Zhang, "Design and Construction of a Rogowski Coil for Measuring Wide Pulsed Current," *IEEE Sensors Journal*, 2011, Vol. 11, No. 1, pp. 123-130, 2011.

[11] Valentinas D, and Hans E, "High-Frequency model of the Rogowski coil with a small number of turns," *IEEE Transaction on Instrumentation and Measurement*, Vol. 56, No. 6, pp. 2284-2289, 2007.

[12] Ha Hengxu, Zhang Baohu, and Lu Zhilai, "The basic theory of boundary protection for EHV transmission lines," *International Conference On Power System Technology Proceedings*, Kunming, China, 2002, pp. 2569-2574.

[13] A. P. Sakis Meliopoulos, and Chien-Hsing Lee, "An alternative method for transient analysis via wavelets," *IEEE Trans. on Power Delivery*, Vol. 15, No. 1, pp. 114-121, 2000.

[14] Zhang Jixian, Zhong Qiuhai, Dai Yaping, "The determination of the threshold and the decomposition order in threshold denoising method based on wavelet transform," *Proceedings of the CSEE*,, Vol. 24, No. 2, pp. 118-122, 2004.

[15] Nan Zhang, and Laden Kezunovic, "Transmission line boundary protection using wavelet transform and neural network," *IEEE Trans. on Power Delivery*, Vol. 22, No. 2, pp. 859-869, 2007.

[16] Ashraf I. Megahed, A. Monem Moussa, and A. E. Bayoumy, "Usage of wavelet transform in the protection of series-compensated transmission lines," *IEEE Trans. on Power Delivery*, Vol. 21, No. 3, pp. 1213-1221, 2006.

[17] XU Qingshan, CHEN Jingen, and TANG Guoqing, "Single ended fault location approach considering bus distributed capacitance effect," *Automation of Electric Power Systems*, Vol. 31, No. 2, pp. 70-73, 2007.

[18] Chui C.K, "An Introduction to Wavelets," *Academic Press,* Boston, USA, 1992.

Zhang Xin He was born in Shanxi, China in 1979. He received his B.S. and M.S. degrees from China University of Mining & Technology in 2002 and 2005, respectively. Now he is a PhD. Candidate in electric power engineering, Tongji University, Shanghai, China.

Mu Longhua He was born in Jiangsu, China in 1963. Currently, he is a professor of Tongji University. His research interests are in power system protection, distribution system automation and power quality.